# SNR Analysis of Time Reversal Signaling on Target and Unintended Receivers in Distributed Transmission

Li Wang, *Senior Member, IEEE*, Ruoguang Li, *Student Member, IEEE*, Chunyan Cao, and Gordon L. Stüber, *Fellow, IEEE*

***Abstract*—This paper analyzes the effect of distributed time-reversal (DTR) transmission scheme on the signal-to-noise ratio (SNR) at its intended and unintended receivers. By focusing the temporal and spatial signal energy on the intended receiver, DTR can effectively maintain a satisfactory SNR level while lowering received signal level at passive eavesdroppers or unintended co-channel users. The DTR performance is analyzed in terms of a SNR gap between the desired and unintended receivers. The SNR gain of DTR is also analyzed over traditional distributed direct transmission and several cooperative beamforming transmission schemes without time-reversal. Numerical results demonstrate the performance improvement of the time-reversal transmission and the validity of our analytical results.**

***Index Terms*—Distributed antenna transmission, time reversal, beamforming, SNR analysis.**

## I. Introduction

TIME REVERSAL (TR) transmission has recently been identified as a promising wireless technology for wide-band multi-path channels because of its inherent ability to focus energy spatially and temporally by exploiting multi-path propagation [1]–[5]. In TR transmissions [2]–[4], the transmitter first acquires the impulse response of its multi-path forward channel response before applying the time-reversed channel impulse response as its signaling pulse over the same channel back to its intended destination receiver. TR effectively exploits the multi-path channel as a natural matched filter such that for destination receivers, at the critical sampling instants, the cumulative signals become focused and the strength becomes very strong. In essence, TR focuses its signal wave at the desired receiver jointly in both the temporal and spatial domains [1]–[5].

In wireless communications, signal leakage to unintended receivers causes security risk and co-channel interference. The signal focusing property of TR can also be exploited to reduce signal leakage to unintended users [6]. TR signaling naturally reduces signal leakage to unintended receivers or unauthorized eavesdroppers, typically at unknown locations, as shown in [7] in a specific indoor test. In terms of PHY secrecy, TR has been shown in [6] to reduce the probability that a signal may be unknowingly intercepted in space and time.

Another interesting study [8] considered how the information theoretic limits on secure communications over multi-path fading channels can be affected by limiting the source to OFDM transmission. The study quantified the PHY secrecy loss if the eavesdropper can utilize a more sophisticated receiver. The techniques used in [8] required knowledge of eavesdropper channel state information (CSI) at the source to derive the secrecy capacity upper bound.

Cooperative beamforming in distributed antennas is another effective technique for a transmitter to concentrate signal power toward the destination. Traditionally, cooperative beamforming considers only the principal path, such as the line-of-sight (LoS) path between each transmit antenna and the destination, despite the presence of multi-path components. In this paper, a distributed time-reversal (DTR) transmission scheme is studied for boosting the source-destination link quality by utilizing both spatial diversity of multiple antennas and the multi-path channel in the temporal domain, while limiting signal leakage to unintended user(s) or passive eavesdropper(s).

DTR precoders can be centrally optimized to minimize information leakage to unintended receivers such as eavesdroppers [9]. The authors of [10] studied the effect of linear block precoding for DTR in the discrete time domain. Given multiple distributed transmit antennas, each "interference-exposed victim" or "eavesdropper" was assumed to have only one antenna. By focusing on block transmission schemes, including OFDMA, their work optimized the precoder and analyzed secrecy capacity by showing that high-rate messages can be transmitted towards an intended user without being decoded by the other users from the viewpoint of information theoretic security. Moreover, the authors of [11] documented an experimental characterization of the confidentiality of an indoor multiple-input single-output TR transmission. An optimized

Manuscript received June 29, 2015; revised December 8, 2015 and March 4, 2016; accepted March 21, 2016. Date of publication March 28, 2016; date of current version May 13, 2016. This work was supported in part by the NSFC of China (Grant 61571056), and in part by the open research fund of the National Mobile Communications Research Laboratory of Southeast University (Grant 2016D04). The associate editor coordinating the review of this paper and approving it for publication was J. Yuan.

Li Wang is with Beijing Key Laboratory of Work Safety Intelligent Monitoring, School of Electronic Engineering, Beijing University of Posts and Telecommunications, Beijing 100876, China, and also with the National Mobile Communications Research Laboratory, Southeast University, Nanjing, China (e-mail: liwang@bupt.edu.cn).

R. Li and C. Cao are with Beijing Key Laboratory of Work Safety Intelligent Monitoring, School of Electronic Engineering, Beijing University of Posts and Telecommunications, Beijing 100876, China.

G. L. Stüber is with the School of Electrical and Computer Engineering, Georgia Institute of Technology, Georgia, GA 30318 USA (e-mail: stuber@ece.gatech.edu).

Color versions of one or more of the figures in this paper are available online at http://ieeexplore.ieee.org.

Digital Object Identifier 10.1109/TCOMM.2016.2547425

precoder design for cooperative amplify-forward relays has been proposed against multiple eavesdroppers [9]. However, such schemes often assume impractical knowledge of the eavesdropper channels or locations, for which a well formulated optimization problem can be solved.

This paper considers a DTR transmission scheme without knowledge of full CSI at the source. By exploiting the frequency selective channel information between each distributed antenna and the destination, each distributed antenna in DTR can apply TR transmission to focus desired signal energy on the critical signal detection time samples at the destination receiver. In doing so, DTR transmission can focus signal energy temporally and spatially in such a manner that the number of distributed transmit antennas can be reduced without much performance degradation. In fact, it was shown in [7] that even the "dumb" receiver demonstrates substantial performance gain using TR signaling.

To the best of the authors' knowledge, the SNR of received DTR signals at both target and unintended receivers has not been analyzed under general multi-path fading channels. Generally, the effects of the delay spread and the number of multi-path channels on signal quality at the destination and unintended receivers have been studied either experimentally or for fixed channels. In particular, for unintended receivers at unknown locations, it is practically difficult to acquire the associated CSI to design optimized DTR precoding. Thus, it is important to evaluate their received signal quality under DTR transmission with CSI knowledge of the destination channel only. Therefore, in order to establish the reduced DTR signal leakage at such unintended receivers, multiple cooperative beamforming transmission schemes shall be analytically evaluated and compared in terms of the SNR at both destination and unintended receivers. The achievable SNR for other comparable distributed beamforming techniques shall also be analyzed, that utilize only the LoS path or a more effective maximum gain path (MGP). LoS distributed beamforming (LoS-DBF) and maximum gain path distributed beamforming (MGP-DBF) both require very simple gain pre-processing at the transmit antenna. DTR, on the other hand, requires that each transmit antenna implements time-reversed pre-filtering. These comparisons can demonstrate the complexity and performance tradeoff.

The superior SNR characteristics of the proposed DTR scheme in this paper shall be demonstrated in the presence of unintended receivers of unknown locations/channels. The proposed DTR transmission scheme only requires local antenna-to-destination CSI at each distributed antenna. Without centralized CSI exchange and control, the effective mitigation of signal leakage through DTR transmission scheme will be established, without CSI knowledge of unintended receiver nodes at the source. Beyond the work of [11] that presents BER test results for QAM-256, this paper analyzes DTR performance with a more general model. The contribution of this paper lies in the novel signal to noise ratio (SNR) analysis at destination and unintended receivers under DTR transmission for random multi-path channels.

The remainder of this paper is organized as follows. Section II presents the system model for analysis and describes the DTR-based transmission scheme. In Section III, the receiver SNR for DTR transmission is analyzed at both the destination and the unintended receivers for channels with fixed number of multi-path components and path-delays. Section IV analyzes the receiver SNR of several more traditional cooperative beamforming strategies. Section V generalizes the SNR analysis for wireless channels with random number of multi-path components and random delays. Section VI presents the numerical results, followed by concluding remarks in Section VII.

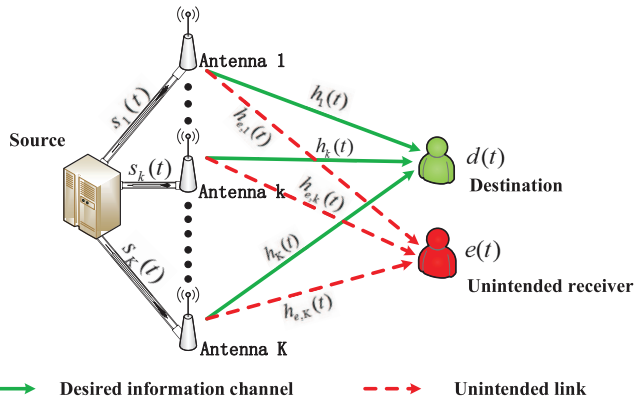


Fig. 1. System model with distributed transmit antennas.

## II. System Model

### A. Cooperative Distributed Antenna Network

A cooperative distributed antenna network is considered as depicted in Fig. 1, where a source wishes to communicate with a distant target receiver with the help of distributed transmit antennas. An unintended receiver is present which may be close to the destination. This paper considers UHF signaling (above 900 MHz), such that the carrier wavelength is very small. For such operating frequencies, in a rich scattering and multi-path channel environment, the coherence distance [15] is in the order of centimeters such that the channels between the distributed antennas and the destination are substantially uncorrelated and different from the channels between the distributed antennas and the unintended receiver (or eavesdropper).

### B. Notations

Consider the notations and symbols below. The system model is characterized by links between the source-to-destination node and source-to-unintended node. The index set of transmit antennas is denoted by $\mathcal{K} = \{1, \ldots, K\}$. The multi-path channel gains are assumed to be independent and identically distributed (i.i.d.) with Rayleigh fading, each with zero mean, i.e., $h_{ki} \sim CN(0, {\sigma_B}^2)$, $h_{e,ki} \sim CN(0, {\sigma_E}^2)$, based on the assumption of a uniform power-delay profile. In other words, $\mathrm{E}\{|h_{ki}|^2\} = \sigma_B^2$, $\mathrm{E}\{|h_{ki}|^4\} = 2\sigma_B^4$, $\mathrm{E}\{h_{ki}\} = \mathrm{E}\{h_{ki}^2\} = 0$. Similarly, $\mathrm{E}\{|h_{e,ki}|^2\} = \sigma_E^2$, $\mathrm{E}\{|h_{e,ki}|^4\} = 2\sigma_E^4$, $\mathrm{E}\{h_{e,ki}\} = \mathrm{E}\{h_{e,ki}^2\} = 0$, Without loss of generality, let $E_p = \int_{-\infty}^{\infty} |p(t)|^2 dt = 1$. Finally, let $\sigma_E = \sigma_B$.

| | |
|---|---|
| $a_m$: | QAM source data symbol in constellation $\mathcal{Q}$; |
| $T$: | QAM symbol duration; |
| $\rho_k(t)$: | normalized pulse for QAM symbol at antenna $k$ |
| $b_k$: | $k-$th antenna power scalar with $\sum_{k=1}^{K} \mathrm{E}\{b_k^2\} = 1$; |
| $h_{ki}$, $h_{e,ki}$: | $i-$th multi-path gain from transmit antenna $k$ to destination and unintended receiver, respectively; |
| $\tau_{ki}$, $\tau_{e,ki}$: | $i-$th multi-path delay from transmit antenna $k$ to destination and unintended receiver, respectively; |
| $T_p$: | maximum multi-path delay; |
| $T_e$, $T_{e0}$, $T_{e1}$: | sampling time at unintended receiver; |
| $L_k + 1$: | number of multi-paths for transmit antenna $k$; |
| $p(t)$: | root raised-cosine receiver filter impulse response; |
| $\sigma_B^2$, $\sigma_E^2$: | variance of i.i.d. delay gains $h_{ki}$ and $h_{e,ki}$, respectively; |
| $P_s$: | transmit power of distributed antennas; |
| $K$: | number of distributed antennas. |
| $C_M^m$: | combinatorial choosing of $m$ objects from $M$ possibilities. |

Two separate cases are considered: initially, $L_k$ is assumed a constant in our basic analysis; later, the collection $\{L_k\}$ is modeled as a set of independent random variables, each with identical uniform distribution $\mathrm{Prob}(L_k = \ell) = L^{-1}, \quad \ell = 0, 1, , \ldots, L-1$. The multi-path delay profile is modeled as exponential over the interval $(0, T_p)$. Specifically, $\tau_{ki}$ and $\tau_{e,ki}$ are assumed to independently follow the truncated exponential density function

$$p_{\tau_{e,ki}}(\tau) = p_{\tau_{ki}}(\tau) = \frac{e^{-\tau/T_0}}{T_0(1 - e^{-T_p/T_0})}[u(\tau) - u(\tau - T_p)]. \tag{1}$$

For uniform power-delay profiles, $T_0 \to \infty$ such that $\tau_{ki}$ and $\tau_{e,ki}$ are uniform between $(0, \ T_p)$.

Note that, the target receiver is synchronized to the incoming signal, whereas the eavesdropper may not be. Without loss of generality, the target receiver samples the received signal at time $T_p$, which is the peak sampling time, whereas the unintended receivers sample their received signals at $T_e$. To give the unintended nodes the benefit of the doubt, the effect of synchronized sampling $T_e = T_p$ will be considered when comparing the received signal qualities later in the paper.

### C. Multi-Path Propagation Model With K Distributed Antennas

The DTR-based transmission is assumed to use time division duplexing (TDD). In TDD systems, channel reciprocity is often assumed for wireless channels of sufficient coherence time. For large enough channel coherence time, channel reciprocity allows each node to assume its transmission channel and reception channel to be the same.

Given channel reciprocity, the DTR transmission scheme consists of two steps. Prior to the transmission, the receiver first sends a pilot signal that allows the transmitter to estimate the impulse response of the multi-path channel from the receiver. Then, the transmitter time-reverses the estimated channel impulse response and uses it to transmit to the receiver through the same channel.

Suppose that each distributed antenna acquires the same symbol $a_m$ via a high speed front-haul network before transmission, and the average symbol power is $P_s = \mathrm{E}\{|a_m|^2\}$. Let $s_k(t)$ denote the transmitted signal from the $k$-th transmit antenna. Assuming QAM symbols, $s_k(t)$ can be written as

$$s_k(t) = b_k \sum_{m=-\infty}^{\infty} a_m \rho_k(t - mT), \quad a_m \in \mathcal{Q} \tag{2}$$

where $b_k$ controls the power distribution of the transmit antenna number $k$ and the waveform $\rho_k(t)$ will be specified later for the various diversity transmission schemes under analysis. The $k-$th average transmission power is $P_k = \frac{1}{T}\int_{-\infty}^{\infty} \mathrm{E}\{|s_k(t)|^2\}dt = \mathrm{E}\{|b_k|^2\}P_s \int_{-\infty}^{\infty} |\rho_k(t)|^2 dt = \mathrm{E}\{|b_k|^2\}P_s$. For simplicity, the waveform $\rho_k(t)$ is normalized to have unit energy $\int_{-\infty}^{\infty} |\rho_k(t)|^2 dt = 1$.

The channel impulse responses from the $k-$th transmit antenna to the destination and the unintended receiver are denoted as $h_k(t)$ and $h_{e,k}(t)$, respectively, each representing a multi-path channel impulse response. The $i-$th path delay from the $k-$th antenna to the destination and the unintended receiver are denoted by $\tau_{ki}$ and $\tau_{e,ki}$, respectively. More specifically, by including the receiver filter response $p(t)$ as part of the channel responses as seen at the transmitter, the two multi-path propagation channels can be described, respectively, as

$$h_k(t) = \sum_{i=0}^{L_k} h_{ki}\, p\,(t - \tau_{ki})\,, \quad h_{e,k}(t) = \sum_{i=0}^{L_k} h_{e,ki}\, p\left(t - \tau_{e,ki}\right), \tag{3}$$

where $i$ denotes the $i-$th path ($i = 0, \ldots, L_k$) and where $L_k + 1$ is the number of channel paths for the $k-$th transmit antenna. Note that $E_p = 1$ and that the average energy of $h_k(t)$ is

$$\begin{aligned} E_k &= \mathrm{E}\left\{\int_{-\infty}^{\infty} |h_k(t)|^2 dt\right\} = \sum_{i=0}^{L_k} \sigma_B^2 \int_{-\infty}^{\infty} |p(t - \tau_{k,i})|^2 dt \\ &= (L_k + 1)\sigma_B^2 E_p = (L_k + 1)\sigma_B^2. \end{aligned} \tag{4}$$

### D. Time-Reversal and Distributed Time-Reversal Transmission

In time-reversal transmission [3], [14], each transmit antenna can utilize its known channel response including the receiver filter to send a (normalized energy) pulse:

$$\rho_k(t) = E_k^{-1/2} h_k^*(T_p - t). \tag{5}$$

To avoid a circular problem of having to define the receiver filter $p(t)$ in order to design time-reversal transmit pulse shape whereas the optimum receiver filter also depends on the transmit pulse shape, the receiver filter at both destination and unintended receivers is chosen to be a simple root-raised cosine (RRC) filter. This offers several distinct advantages: (i) the RRC

receiver filter is not channel dependent; (ii) the RRC receiver filter can be optimum when there is no multi-path distortion; (iii) the RRC filter can keep the $T-$spaced output noise samples white.

By using time-reversal transmission, antenna $k$ now transmits a new signal that is of the form

$$s_k^{DTR}(t) = b_k \sum_{m=-\infty}^{\infty} \frac{a_m}{\sqrt{E_k}} h_k^*(T_p - t + mT). \tag{6}$$

Recall that $P_s = \mathrm{E}\{|a_m|^2\}$. The normalization makes it simpler to control power distribution by adjusting $b_k$. Given $K$ antennas, $b_k = 1/\sqrt{K}$ allows equal gain transmission (EGT) in DTR by exploiting only local CSI [16].

The delay $T_p$ must be large enough to account for the maximum multi-path delay spread among all transmitting antennas. Let $*$ denote discrete convolution. Before sampling, the signals at the RRC receiver filter output from the $k-$th antenna at the destination and unintended receivers are, respectively,

$$d_k(t) = s_k^{DTR}(t) * h_k(t) + n_k(t), \tag{7a}$$

$$e_k(t) = s_k^{DTR}(t) * h_{e,k}(t) + n_{e,k}(t). \tag{7b}$$

For convenience, define the received pulse at the destination as

$$\begin{aligned} q_k(t) &= h_k^*\left(T_p - t\right) * h_k(t)/E_k^{1/2} \\ &= \sum_{i=0}^{L_k}\sum_{\ell=0}^{L_k} \frac{h_{ki}h_{k\ell}^*}{\sqrt{E_k}} \int_{-\infty}^{\infty} p(v-\tau_{ki})p^*(T_p - t + v - \tau_{k\ell})dv. \end{aligned} \tag{8}$$

On the other hand, at the unintended receiver define the received pulse $q_{e,k}(t)$ as

$$\begin{aligned} q_{e,k}(t) &= h_k^*\left(T_p - t\right) * h_{e,k}(t)/E_k^{1/2} \\ &= \sum_{i=0}^{L_k}\sum_{\ell=0}^{L_k} \frac{h_{e,ki}h_{k\ell}^*}{\sqrt{E_k}} \\ &\quad \cdot \int_{-\infty}^{\infty} p(v-\tau_{e,ki})p^*(T_p - t + v - \tau_{k\ell})dv. \end{aligned} \tag{9}$$

Now that the received signal pulse-shaping from time-reversal transmission have been specified, the two received signals from a given transmit antenna can be rewritten as

$$d_k(t) = b_k \sum_{m=-\infty}^{\infty} a_m q_k(t - mT) + n_k(t), \tag{10a}$$

$$e_k(t) = b_k \sum_{m=-\infty}^{\infty} a_m q_{e,k}(t - mT) + n_{e,k}(t). \tag{10b}$$

It is important to note that the equivalent receiver filter output pulse for TR transmission at the destination has a maximum-power peak at time $t = T_p$,

$$q_k(T_p) = \frac{1}{\sqrt{E_k}} \int_{-\infty}^{\infty} \left| \sum_{i=0}^{L_k} h_{ki}\, p(v - \tau_{ki}) \right|^2 dv. \tag{11}$$

This peak sampling property does not hold, however, for the unintended receiver node.

### *E. Analysis of SNR Enhancement by DTR*

Notice that DTR transmission focuses signal energy at the critical sampling instants based on the overall source-to-destination channel awareness. The focused signal energy leads to a substantial SNR improvement at sampling time instants and better signal quality at the destination, but not necessarily so for the unintended receiver whose channels are uncorrelated with destination's. The objective of this paper is to analyze how this important energy focusing property of DTR transmission can significantly increase the performance gap between the intended and unintended receivers.

Specifically, the SNR of the $T$-spaced samples at the output of the receiver filter at the destination receiver is substantially higher than the SNR of the $T$-spaced samples at output of the receiver filter at the unintended receiver. For practical purpose, if DTR transmission can significantly increase the SNR at the desired receiver while keeping the SNR at the unintended receivers at unknown locations sufficiently low, then it can ensure good source-destination link performance while reducing co-channel interference to other nearby links. Moreover, a large SNR gap between the source-destination and source-unintended receiver links can likewise protect information from being decoded by passive eavesdroppers at locations unknown to the transmitter.

The receiver-dependent SNR may be translated into a corresponding secrecy rate, which is the maximum achievable data rate at the target receiver without being intercepted by eavesdropper, by importing the SNR into the traditional secrecy rate formula as discussed in [17]–[19]. For a unit bandwidth, the secrecy rate $R_s$ is given by

$$R_s = \left[\log_2(1 + \mathrm{SNR}_d) - \log_2(1 + \mathrm{SNR}_e)\right]^+, \tag{12}$$

where $\mathrm{SNR}_d$ and $\mathrm{SNR}_e$ are the SNR at the destination and the unintended receivers, respectively.

It is of little practical interest to derive the secrecy rate $R_s$ for a specific set of channel impulse responses. For practical utility, it is more meaningful to investigate the DTR performance for a typical class of random channels by determining the mean secrecy rate $\mathrm{E}\{R_s\}$ over the ensemble of such random channels. However, since the secrecy rate is a nonlinear function of both $\mathrm{SNR}_d$ at the destination and $\mathrm{SNR}_e$ at the unintended receiver [17], [18], the ensemble averaged secrecy rate cannot be evaluated based on average received SNR values. Consequently, the respective SNR at the destination and the unintended receiver shall be analytically derived to characterize the benefits of DTR transmission. To obtain results that are meaningful and practical, the average SNR over an ensemble of random multi-path channels (including the number of multi-paths) shall be considered. As discussed later, perfect equalization at the intended and unintended receivers is assumed to cancel any inter-symbol interference (ISI) when determining the received SNR [7]. Alternatively, pre-equalization at the source [12], [13] can be used for effective ISI removal at the cost of higher transmitter complexity.

Our analytical results and the accompanied numerical evaluation will demonstrate that DTR can achieve lower co-channel

interference and a more degraded SNR at passive eavesdroppers than traditional distributed beamforming (DBF). To be fair, the receivers are assumed to be ideal with perfect equalization for either the DTR or DBF transmission schemes. Such ideal receivers with perfect equalization will provide a performance benchmark for the various transmission schemes under consideration. By utilizing the individual channel information from each distributed antenna to the destination, DTR will be shown to achieve the same level of SNR-gap (or secrecy rate) but with a fewer number of distributed transmit antennas than LoS-DBF.

## III. Analysis of Distributed Time-Reversal

### A. DTR Reception and Analytical Assumptions

Let the additive white Gaussian noise at the destination and the unintended receiver be denoted as $n(t)$ and $n_e(t)$, respectively. Since all $K$ antennas perform the same functionality and transmit the same symbol $a_m$, the received signals at the two receivers are, respectively,

$$d(t) = \sum_{k=1}^{K} d_k(t) = \sum_m a_m \sum_{k=1}^{K} b_k q_k(t - mT) + n(t), \quad (13a)$$

$$e(t) = \sum_{k=1}^{K} e_k(t) = \sum_m a_m \sum_{k=1}^{K} b_k q_{e,k}(t - mT) + n_e(t). \quad (13b)$$

Recall that for the destination receiver, the peak SNR sampling instants are at $t_\ell = \ell T + T_p$. The noise inputs $n(t)$ and $n_e(t)$ to the receiver filters are additive white Gaussian random processes with power spectral densities $\sigma_n^2$ and $\sigma_e^2$, respectively. Since $p(t)$ is chosen as the well known RRC filter response, the $T-$spaced noise samples $n(\ell T + T_p)$ and $n_e(\ell T + T_e)$ taken at time intervals of $\ell T$ are independent Gaussian random variables [15], [20].

An ideal receiver is assumed at both destination and eavesdropoper. Unlike traditional secrecy analysis that focuses on discrete channel models, our model is the practical analog signal model. To investigate the secrecy effect, idealistic receivers are assumed at both the destination and unintended receiver when determining the secrecy rate. In particular, it is assumed that

- Both destination and unintended receiver have CSI from each distributed antenna to their respective receivers.
- Both destination and unintended receivers have a RRC front-end filter whose output is periodically sampled.
- Both destination and unintended receiver are capable of designing **an ideal and perfect receiver** to remove all ISI from their sampled RRC filter output signals.

### B. Received SNR Analysis Under DTR-Based Transmission

Recall that for the destination receiver, the peak SNR occurs at the sampling instants $t_\ell = \ell T + T_p$ where the peak pulse magnitude is obtained. However, for the unintended receiver, there may not be best sampling instants because of the random multi-path channels $h_{e,ki}$ and $h_{ki}$ involved. Hence, the unintended receiver or eavesdropper samples the RRC filter output with the same period $T$ but with an arbitrary time offset $T_e$, i.e., samples are taken at times $t_\ell^{(e)} = \ell T + T_e$. Thus, the two received signals after sampling are

$$d(t_\ell) = \sum_m a_m \sum_{k=1}^{K} b_k q_k(t_\ell - mT) + n(t_\ell), \quad (14a)$$

$$e(t_\ell^{(e)}) = \sum_m a_m \sum_{k=1}^{K} b_k q_{e,k}(t_\ell^{(e)} - mT) + n_e(t_\ell^{(e)}). \quad (14b)$$

Note that $d(t_\ell)$ and $e(t_\ell^{(e)})$ are used to detect symbol $a_\ell$. Clearly, both destination and unintended receiver have to contend with ISI [21] at the receiver. The idealistic scenario will be considered, in which the destination receiver can acquire the full channel information with respect to $\sum_{k=1}^{K} b_k q_k(t - mT)$ such that all ISI at the receiver can be eliminated effectively through the use of a decision feedback equalizer without causing detection performance degradation [22]. At the transmitter, pre-equalization [12], [13] can also achieve effective ISI removal at higher transmitter complexity.

Perfect equalization and perfect CSI are impractical in actual communication systems. Residual ISI may result in receiver performance loss. However, the effect of unmitigated ISI at both the destination receiver and the unintended receivers varies with the channel delay profile, the length and type of pilot symbols, and the types of channel estimation and equalization algorithms, among other factors. Characterization of residual ISI effect would be system-dependent. Hence, this study focuses on investigating the best case scenario of perfect ISI suppression to provide a design benchmark. By establishing performance limit in terms of the received signal SNR, our results can provide useful design guidelines. Practitioners can develop additional ISI margins from measurement and experience.

### C. Average SNR

For the $\ell-$th QAM symbol, the receiver output (corresponding to the input $d(t_\ell)$) is given by

$$a_\ell \sum_k b_k q_k(T_p) = a_\ell \sum_k \beta_k \int_{-\infty}^{\infty} \left| \sum_{i=0}^{L_k} h_{ki}\, p(v - \tau_{ki}) \right|^2 dv,$$

where $\beta_k = b_k/\sqrt{E_k}$. Note that the QAM symbol $a_\ell$ has zero mean and average power $P_s = E\{|a_m|^2\}$. Since the noise $n(t_\ell)$ is $\mathcal{CN}(0, \sigma_n^2)$, the general expression of the received signal-to-noise ratio for the destination is given by

$$\mathrm{SNR}_d = \frac{P_s}{\sigma_n^2} \mathrm{E}\left\{ \left[ \sum_k \beta_k \int_{-\infty}^{\infty} \left| \sum_{i=0}^{L_k} h_{ki}\, p(v - \tau_{ki}) \right|^2 dv \right]^2 \right\}. \quad (15)$$

To analyze the SNR, recall that the complex multi-path channel gains associated with the different transmit antennas and delays $\{h_{ki}\}$ are independent zero-mean complex Gaussian random variables with $\mathrm{E}\{|h_{ki}|^2\} = \sigma_B^2$, $\mathrm{E}\{|h_{ki}|^4\} = 2\sigma_B^4$, and $\mathrm{E}\{h_{ki}\} =$

$E\{h_{ki}^2\} = 0$. Thus,

$$\begin{aligned} Q_{d1} =& \ \mathrm{E}\left\{\left[\sum_k \beta_k \int_{-\infty}^{\infty}\left|\sum_{i=0}^{L_k} h_{ki}\, p(v-\tau_{ki})\right|^2 dv\right]^2\right\} \\ =& \ \mathrm{E}\left\{\sum_{k_1}\beta_{k1}\int_v\left(\sum_{i_1=0}^{L_{k_1}} h_{k_1 i_1}\, p(v-\tau_{k_1 i_1})\right.\right. \\ & \left.\cdot\sum_{i_2=0}^{L_{k_1}} h_{k_1 i_2}^* p^*(v-\tau_{k_1 i_2})\right) dv \\ & \times\sum_{k_2}\beta_{k2}\int_w\left(\sum_{j_1=0}^{L_{k_2}} h_{k_2 j_1}\, p(w-\tau_{k_2 j_1})\right. \\ & \left.\left.\cdot\sum_{j_2=0}^{L_{k_2}} h_{k_2 j_2}^* p^*(w-\tau_{k_2 j_2})\right) dw\right\}. \end{aligned} \tag{16}$$

Let us define

$$\begin{aligned} E_p &= \int_v |p(v-\tau)|^2\, dv = 1 \quad \text{and} \\ R_p(\tau_1-\tau_2) &= \int_v p(v-\tau_1)p^*(v-\tau_2)dv. \end{aligned} \tag{17a}$$

Using the i.i.d. property of $\{h_{ki}\}$ gives

$$\begin{aligned} Q_{d1} =& \int_v\int_w\left[\sum_k \beta_k^2\left(\sum_{i,j,i\neq j}^{L_k}\sigma_B^4\,|p(v-\tau_{ki})|^2\,|p(w-\tau_{kj})|^2\right.\right. \\ & +\sum_i^{L_k} 2\sigma_B^4\,|p(v-\tau_{ki})|^2\,|p(w-\tau_{ki})|^2 \\ & +\sum_{i_1,i_2,i_2\neq i_1}^{L_k}\sigma_B^4 p(v-\tau_{ki_1})p^*(v-\tau_{ki_2}) \\ & \left.\cdot(w-\tau_{ki_2})p^*(w-\tau_{ki_1})\right)+\sum_{k_1}\sum_{k_2\neq k_1}\beta_{k1}\beta_{k2} \\ & \left.\cdot\left(\sum_{i,j}^{L_{k_1},L_{k_2}}\sigma_B^4\left|p(v-\tau_{k_1 i})\right|^2\left|p(w-\tau_{k_2 j})\right|^2\right)\right] dv\,dw \\ =& \ \sigma_B^4\left(\sum_k \beta_k(L_k+1)\right)^2 \\ & +\sigma_B^4\sum_k\beta_k^2\sum_{i_1=0}^{L_k}\sum_{i_2=0}^{L_k}|R_p(\tau_{ki_1}-\tau_{ki_2})|^2. \end{aligned} \tag{17b}$$

Recall that $\beta_k = (\sqrt{K(L_k+1)}\sigma_B)^{-1}$. Thus,

$$\begin{aligned} Q_{d1} =& \ \sigma_B^2\frac{1}{K}\left(\sum_k\sqrt{(L_k+1)}\right)^2 + \\ & \frac{\sigma_B^2}{K}\sum_k\frac{1}{(L_k+1)}\sum_{i_1=0}^{L_k}\sum_{i_2=0}^{L_k}|R_p(\tau_{ki_1}-\tau_{ki_2})|^2. \end{aligned} \tag{17c}$$

On the other hand, the unintended receiver will sample at time $T_e$ to yield output sample

$$\begin{aligned} q_{e,k}(T_e) =& \frac{1}{\sqrt{E_k}}\int\sum_{i=0}^{L_k} h_{e,ki}\, p(v-\tau_{e,ki}) \\ & \cdot\sum_{j=0}^{L_k} h_{kj}^* p^*(T_p-T_e+v-\tau_{e,kj})dv, \end{aligned} \tag{18}$$

whose SNR is

$$\mathrm{SNR}_e = \frac{P_s}{\sigma_e^2}\mathrm{E}\left\{\left|\sum_{k=1}^{K} b_k q_{e,k}(T_e)\right|^2\right\}. \tag{19}$$

Therefore, for a given $L_k$,

$$\begin{aligned} Q_{e1} =& \ \mathrm{E}\left\{\left|\sum_{k=1}^{K} b_k q_{e,k}(T_e)\right|^2\right\} \\ =& \ \mathrm{E}\left\{\sum_{k_1}\beta_{k1}\int_v\sum_{i_1=0}^{L_{k_1}} h_{e,k_1 i_1}\, p(v-\tau_{e,k_1 i_1})\right. \\ & \cdot\sum_{i_2=0}^{L_{k_1}} h_{k_1 i_2}^* p^*(T_p-T_e+v-\tau_{k_1 i_2})dv \\ & \times\sum_{k_2}\beta_{k2}\int_w\sum_{j_1=0}^{L_{k_2}} h_{e,k_2 j_1}^* p^*(w-\tau_{e,k_2 j_1}) \\ & \left.\cdot\sum_{j_2=0}^{L_{k_2}} h_{k_2 j_2}\, p(T_p-T_e+w-\tau_{k_2 j_2})dw\right\} \\ =& \int_v\int_w\sum_k\beta_k^2\left[\sum_{i=0}^{L_k}\sum_{j=0}^{L_k}\mathrm{E}\left\{h_{e,ki}h_{e,ki}^* h_{kj}h_{kj}^*\right\}\right. \\ & p(v-\tau_{e,ki})p(T_p-T_e+v-\tau_{kj}) \\ & \left.\cdot p^*\left(T_p-T_e+w-\tau_{kj}\right)p^*(w-\tau_{e,ki})\right]dv\,dw \\ =& \sum_k\beta_k^2\sum_{i,j}\sigma_B^2\sigma_E^2|R_p(T_p-T_e-\tau_{kj}+\tau_{e,ki})|^2 \quad (20a) \\ =& \frac{\sigma_E^2}{K}\sum_k\frac{1}{(L_k+1)}\sum_{i,j}R_p(T_p-T_e-\tau_{kj}+\tau_{e,ki})|^2. \end{aligned}$$

(20b)

Hence, given $L_k+1$ multi-paths for each antenna, the SNR at the destination and the unintended receiver can be found, respectively, as

$$\mathrm{SNR}_{d1} = \frac{P_s Q_{d1}}{\sigma_n^2} \quad \text{and} \quad \mathrm{SNR}_{e1} = \frac{P_s Q_{e1}}{\sigma_e^2}. \tag{21}$$

Based on the above analysis, the SNR-gap between the intended and unintended receivers in DTR can be evaluated as $\mathrm{SNR}_{gap1}(\mathrm{dB}) = \mathrm{SNR}_{d1}(\mathrm{dB}) - \mathrm{SNR}_{e1}(\mathrm{dB})$. Naturally, one can also quantify the resulting secrecy rate per unit bandwidth [17], [18] $\left[\log(1+\mathrm{SNR}_{d1}) - \log(1+\mathrm{SNR}_{e1})\right]^+$ based on (12).

### D. Equal Gain Transmission in DTR

Our analytical results depend on the power distribution among transmit antennas $b_k$. Typically, the source central controller is not required to be aware of each antenna's channel gain. To avoid the complexity of centralized control and exchange of channel knowledge among antennas, equal power distribution can be applied among the transmit antennas. Thus, given $K$ total antennas, the weights $b_k = 1/\sqrt{K}$ and $\beta_k = 1/\sqrt{K E_k}$ can be used to achieve equal gain transmission (EGT) in DTR unless otherwise specified. Since $E_k = (L_k + 1)\sigma_B^2$, $Q_{d1}$ and $Q_{e1}$ of (21) can be directly evaluated for EGT.

## IV. Analysis of Classic Transmission Schemes

Using the same method as the one described in Section III for DTR, this section derives the secrecy rate of direct transmission, and beamforming in distributed antenna networks.

### A. Direct Transmission (DT)

In naïve direct transmission, each antenna sends the same pulse $\rho_k(t) = p^*(T_p - t)$ matched to the receiver RRC filter. Note that the pulse has energy $E_p = 1$. Recall that the received signals at the destination and unintended receivers from the $k$th transmit antenna are, respectively,

$$d_k(t) = b_k \sum_{m=-\infty}^{\infty} a_m \rho_k(t - mT) * h_k(t) + n_k(t), \tag{22a}$$

$$e_k(t) = b_k \sum_{m=-\infty}^{\infty} a_m \rho_k(t - mT) * h_{e,k}(t) + n_{e,k}(t). \tag{22b}$$

Let us define the two combined responses

$$\bar{z}_k(t) = h_k(t) * p^*(T_p - t), \tag{23a}$$

$$\bar{z}_{e,k}(t) = h_{e,k}(t) * p^*(T_p - t). \tag{23b}$$

Thus, the signals received at the destination and the unintended receiver can be expressed, respectively, as

$$d(t) = \sum_{k=1}^{K} d_k(t) = \sum_m a_m \sum_{k=1}^{K} b_k \bar{z}_k(t - mT) + n(t), \tag{24a}$$

$$e(t) = \sum_{k=1}^{K} e_k(t) = \sum_m a_m \sum_{k=1}^{K} b_k \bar{z}_{e,k}(t - mT) + n_e(t). \tag{24b}$$

The peak SNR sampling times for the destination and the unintended receiver are $t_\ell = T_p + \ell T$ and $T_{e0} + \ell T$, respectively. At the points of sampling and detection,

$$\bar{z}_k(T_p) = \sum_{i=0}^{L_k} h_{ki} \int_{-\infty}^{\infty} p(v - \tau_{ki}) p^*(v) dv = \sum_{i=0}^{L_k} h_{ki} R_p(\tau_{ki}), \tag{25a}$$

$$\begin{aligned} \bar{z}_{e,k}(T_{e0}) &= \sum_{i=0}^{L_k} h_{e,ki} \int_{-\infty}^{\infty} p(v - \tau_{e,ki}) p^*(T_p - T_{e0} + v) dv \\ &= \sum_{i=0}^{L_k} h_{e,ki} R_p(T_p - T_{e0} + \tau_{e,ki}). \end{aligned} \tag{25b}$$

The signal energy at the destination receiver at the sampling instant $t_\ell = T_p + \ell T$ is

$$Q_{d2} = \mathrm{E}\left\{ \left| \sum_k b_k \bar{z}_k(T_p) \right|^2 \right\} = \sum_k {b_k}^2 \sum_{i=0}^{L_k} \sigma_B^2 \left| R_p(\tau_{ki}) \right|^2, \tag{26a}$$

while at the unintended receiver, the signal energy at the sampling instant $T_{e0} + \ell T$ is

$$\begin{aligned} Q_{e2} &= \mathrm{E}\left\{ \left| \sum_k b_k \bar{z}_{e,k}(T_{e0}) \right|^2 \right\} \\ &= \sum_k {b_k}^2 \sum_{i=0}^{L_k} \sigma_E^2 \left| R_p(T_p - T_{e0} + \tau_{e,ki}) \right|^2. \end{aligned} \tag{26b}$$

Given the $L_k + 1$ multi-paths for each transmit antenna, the SNRs at destination and unintended receiver are, respectively,

$$\mathrm{SNR}_{d2} = \frac{P_s Q_{d2}}{\sigma_n^2}, \quad \text{and} \quad \mathrm{SNR}_{e2} = \frac{P_s Q_{e2}}{\sigma_e^2}. \tag{27}$$

The SNR gap and the resulting secrecy rate can be quantified directly. For the most common case, equal gain transmission weights $b_k = 1/\sqrt{K}$ can be used to evaluate the SNR and SNR gap of (27) numerically.

### B. Distributed Beamforming

Cooperative beamforming is a widely used method to enhance the security of communications, where transmit antennas utilize distributed beamforming to concentrate the signal towards the intended destination and mitigate the information leakage to an unintended receiver.

Distributed beamforming usually considers only a single path between a transmit antenna and the destination, while in practice the signals transmitted by the transmit antennas propagate through multi-path channels and the received signals at the unintended receiver(s) may not fully achieve coherent combining. Therefore, the achievable SNR for distributed beamforming will be analyzed considering both the one-path model and a practical multi-path channel model.

With distributed beamforming, the $k$th transmit antenna uses the (normalized) pulse

$$\rho_k(t) = p^*(T_p - \tau_{ki_0} - t),$$

where

$$i_0 = \begin{cases} \arg \max\limits_{0 \le i \le L_k} |h_{ki}^*|, & \text{MGP}, \\ 0, & \text{Direct LoS}. \end{cases}$$

For Maximum Ratio Transmission (MRT) [23], each antenna adopts a different gain $b_k = h_{ki_0}^*/\zeta$, thereby transmitting $b_k p^*(T_p - \tau_{ki_0} - t)$. Since $h_{ki}$ is a random variable, $\arg\max_i |h_{ki}^*|$ is a special kind of random variable that requires order statistics [24]. Here $\zeta$ is used to normalize $\sum_1^K E\{|b_k|^2\} = 1$ for fairness.

In distributed beamforming, two different types of beamforming are considered for comparison:

- **LoS-DBF:** With line of sight beamforming, each transmit antenna sends a pulse $h_{k0}^* p^*(T_p - \tau_{k0} - t)/(\sigma_B\sqrt{K})$ that is matched to the first LoS delay only.
- **MGP-DBF:** With maximum gain path distributed beamforming, at each transmit antenna the strongest multipath component is selected for distributed beamforming. Similar to LoS-DBF, each antenna sends a pulse $h_{ki_0}^* p^*(T_p - \tau_{ki_0} - t)/\zeta$ that is matched to the strongest delay path $i_0$ only.
  Order statistics can be used to determine the $b_k$. For $X_1, X_2, \ldots, X_n$ i.i.d. continuous random variables with probability density function (PDF) $f(x)$ and cumulative distribution function (CDF) $F(x)$, the PDF of the maximum is $f_{(n)}(x) = nf(x)F(x)^{n-1}$ [24]. Recall that $x_k = |h_{ki}^*|^2$ is a random variable following the exponential distribution [15]. Therefore, denoting $i_0 = \arg\max_i |h_{ki}|$, yields

$$f_{|h_{ki_0}^*|^2}(x) = (L_k+1)\frac{1}{\sigma_B^2}\exp\left(-\frac{x}{\sigma_B^2}\right)\left(1-\exp\left(\frac{-x}{\sigma_B^2}\right)\right)^{L_k}, \quad \text{where} \quad x \geq 0. \tag{28a}$$

$$\begin{aligned}\mathrm{E}(|b_k|^2) &= \frac{1}{\zeta^2}\int_0^\infty x f_{(n)}(x)dx \\ &= \frac{\sigma_B^2}{\zeta^2}(L_k+1)\sum_{i=0}^{L_k} C_{L_k}^i(-1)^i \\ &\quad \cdot \int_0^\infty t\exp[-(i+1)t]dt \\ &= \frac{\sigma_B^2}{\zeta^2}(L_k+1)\sum_{i=0}^{L_k} C_{L_k}^i(-1)^i(i+1)^{-2} \\ &= \sigma_B^2\zeta^{-2}G_0,\end{aligned}$$

$$\text{where} \quad G_0(L_k) = (L_k+1)\sum_{i=0}^{L_k} C_{L_k}^i(-1)^i(i+1)^{-2}. \tag{28b}$$

Therefore, in MGP-DBF the normalization factor $\zeta = \sigma_B\sqrt{KG_0(L_k)}$ is used.

### C. Analysis

With DBF, $K$ antennas cooperatively transmit their signals to the destination. Considering that the unintended receiver's channel information is unknown, with DBF the received signals at the destination and the unintended receiver from the $k-$th transmit antenna can be described as

$$d_k(t) = b_k\sum_m a_m h_k(t-mT) * p^*(T_p - \tau_{ki_0} - t) + n_k(t), \tag{29a}$$

$$e_k(t) = b_k\sum_m a_m h_{e,k}(t-mT) * p^*(T_p - \tau_{ki_0} - t) + n_{e,k}(t). \tag{29b}$$

For convenience, define

$$\begin{aligned}\bar{g}_k(t) &= h_k(t) * p^*(T_p - \tau_{ki_0} - t) \\ &= \sum_i^{L_k} h_{ki}\int_{-\infty}^\infty p(v-\tau_{ki})p^*(T_p - \tau_{ki_0} - t + v)dv,\end{aligned} \tag{30a}$$

$$\begin{aligned}\bar{g}_{e,k}(t) &= h_{e,k}(t) * p^*(T_p - \tau_{ki_0} - t) \\ &= \sum_i^{L_k} h_{e,ki}\int_{-\infty}^\infty p(v-\tau_{e,ki})p^*(T_p - \tau_{ki_0} - t + v)dv.\end{aligned} \tag{30b}$$

When $K$ antennas cooperatively transmit to the destination via DBF, the received signals at the destination and the unintended receiver can be written as, respectively,

$$d(t) = \sum_{k=1}^K d_k(t) = \sum_m a_m\sum_{k=1}^K b_k\bar{g}_k(t-mT) + n(t), \tag{31a}$$

$$e(t) = \sum_{k=1}^K e_k(t) = \sum_m a_m\sum_{k=1}^K b_k\bar{g}_{e,k}(t-mT) + n_e(t). \tag{31b}$$

Let the peak SNR sampling times for the destination and the unintended receiver be $t_\ell = T_p + \ell T$ and $T_{e1} + \ell T$, respectively. It follows that

$$\begin{aligned}Q_{d3} &= \mathrm{E}\left\{\left|\sum_{k=1}^K b_k\bar{g}_k(T_p)\right|^2\right\} \\ &= \mathrm{E}\left\{\sum_{k_1}\frac{h_{k_1i_0}^*}{\zeta}\sum_i^{L_{k_1}} h_{k_1i}\int_{-\infty}^\infty p(v-\tau_{k_1i})p^*(v-\tau_{k_1i_0})dv\right. \\ &\quad \left.\times\sum_{k_2}\frac{h_{k_2i_0}}{\zeta}\sum_j^{L_{k_2}} h_{k_2j}^*\int_{-\infty}^\infty p^*(w-\tau_{k_2j})p(w-\tau_{k_2i_0})dw\right\},\end{aligned} \tag{32a}$$

$$\begin{aligned}Q_{e3} &= \mathrm{E}\left\{\left|\sum_{k=1}^K b_k\bar{g}_{e,k}(T_{e1})\right|^2\right\} \\ &= \mathrm{E}\left\{\sum_{k_1}\frac{h_{k_1i_0}^*}{\zeta}\sum_i^{L_{k_1}} h_{e,k_1i}\right. \\ &\quad \cdot\int_{-\infty}^\infty p(v-\tau_{e,k_1i})p^*(T_p+v-T_{e1}-\tau_{k_1i_0})dv \\ &\quad \cdot\sum_{k_2}\frac{h_{k_2i_0}}{\zeta}\sum_j^{L_{k_2}} h_{e,k_2j}^* \\ &\quad \left.\cdot\int_{-\infty}^\infty p^*(w-\tau_{e,k_2j})p(T_p+w-T_{e1}-\tau_{k_1i_0})dw\right\}.\end{aligned} \tag{32b}$$

*1) LoS-DBF:* For direct LoS beamforming, $i_0 = 0$ and $\zeta = \sigma_B\sqrt{K}$ such that

$$Q_{d3} = \frac{1}{K}\sum_{k1}\sum_{k2\neq k1}\sigma_B^2|E_p|^2 + \frac{1}{K}\sum_k\left(\sum_{i\neq i_0}\sigma_B^2|R_p(\tau_{ki}-\tau_{ki_0})|^2 + 2\sigma_B^2|E_p|^2\right)$$
$$= \sigma_B^2(K+1) + \frac{1}{K}\sum_k\left(\sum_{i\neq 0}\sigma_B^2|R_p(\tau_{ki}-\tau_{k0})|^2\right), \tag{33a}$$

$$Q_{e3} = \frac{1}{K}\sum_k\left(\sum_i\sigma_E^2|R_p(T_p - T_{e1} - \tau_{k0} + \tau_{e,ki})|^2\right). \tag{33b}$$

When considering $L_k + 1$ multi-paths for each transmit antenna, the SNRs at the destination and the unintended receiver are, respectively,

$$\mathrm{SNR}_{d3} = \frac{P_s Q_{d3}}{\sigma_n^2},\ \mathrm{SNR}_{e3} = \frac{P_s Q_{e3}}{\sigma_n^2}. \tag{33c}$$

*2) MGP-DBF:* For MGP distributed beamforming, recall that $i_0 = \arg\max_i |h_{ki}|$ such that $b_k = h_{ki_0}^*/(\sigma_B\sqrt{KG_0})$. Using the pdf in (28a) gives

$$\mathrm{E}(|b_k|^4) = \frac{1}{\sigma_B^4K^2G_0(L_k)^2}\int_0^\infty x^2 f_{(n)}(x)dx$$
$$= \frac{1}{[KG_0(L_k)]^2}(L_k+1)\sum_{i=0}^{L_k}C_{L_k}^i(-1)^i \cdot\int_0^\infty t^2\exp[-(i+1)t]dt$$
$$= K^{-2}G_1(L_k), \tag{34a}$$

where

$$G_1(L_k) = \frac{(L_k+1)}{[G_0(L_k)]^2}2\sum_{i=0}^{L_k}C_{L_k}^i(-1)^i(i+1)^{-3} = (L_k+1)^{-1}\frac{2\sum_{i=0}^{L_k}C_{L_k}^i(-1)^i(i+1)^{-3}}{\left[\sum_{i=0}^{L_k}C_{L_k}^i(-1)^i(i+1)^{-2}\right]^2}. \tag{34b}$$

Therefore,

$$Q_{d4} = \mathrm{E}\left\{\left|\sum_{k=1}^K b_k\bar{g}_k(T_p)\right|^2\right\}$$
$$= \sum_k\sigma_B^2\left(\sum_{i\neq i_0}\mathrm{E}\{|b_k|^2\}|R_p(\tau_{ki}-\tau_{ki_0})|^2 + G_0K\mathrm{E}\{|b_k|^4)\}\right) + \sum_{k1}\sum_{k2\neq k1}\sigma_B^2KG_0\mathrm{E}\{|b_{k1}|^2\}\mathrm{E}\{|b_{k2}|^2\}$$
$$= K^{-1}\sigma_B^2\sum_k\left(\sum_{i\neq i_0}|R_p(\tau_{ki}-\tau_{ki_0})|^2\right) + G_1(L_k)G_0(L_k)\sigma_B^2 + (K-1)G_0(L_k)\sigma_B^2, \tag{35a}$$

$$Q_{e4} = K^{-1}\sigma_E^2\sum_k\left(\sum_i|R_p(T_p - T_{e1} - \tau_{ki_0} + \tau_{e,ki})|^2\right). \tag{35b}$$

The SNRs at the destination and the unintended receiver are, respectively,

$$\mathrm{SNR}_{d4} = \frac{P_s Q_{d4}}{\sigma_n^2},\ \mathrm{SNR}_{e4} = \frac{P_s Q_{e4}}{\sigma_e^2}. \tag{36}$$

## V. Random Delay Analysis

The more general and practical wireless scenario is now considered, where the number of multi-paths per transmit antenna $(L_k + 1)$ and their respective multi-path delays are randomly uniformed. As mentioned in Section II, this scenario captures the uncertain multi-path environment.

### A. DTR Transmission Analysis

For DTR transmission, an average can be taken over the $L_k$ to obtain

$$\mathrm{E}_{L_k}\{Q_{d1}\} = \sigma_B^4\mathrm{E}\left\{\sum_k\beta_k^2[(L_k+1)L_k + 2(L_k+1)] + \sum_{k_1}\sum_{k_2\neq k_1}\beta_{k1}\beta_{k2}(L_{k_1}+1)(L_{k_2}+1) + \sum_k\beta_k^2\sum_{i_1=0}^{L_k}\sum_{i_2\neq i_1}^{L_k}|R_p(\tau_{ki_1}-\tau_{ki_2})|^2\right\}$$
$$= \sigma_B^2\sum_k b_k^2\left(\frac{3+L}{2}\right) + \sigma_B^2\left(\frac{1}{L}\sum_{L_k=0}^{L-1}\sqrt{L_k+1}\right)^2\sum_{k_1}\sum_{k_2\neq k_1}b_{k1}b_{k2} + \sigma_B^2\sum_k b_k^2\frac{1}{L}\sum_{L_k=0}^{L-1}\frac{1}{L_k+1} \cdot\sum_{i_1=0}^{L_k}\sum_{i_2\neq i_1}^{L_k}\mathrm{E}\left\{|R_p(\tau_{ki_1}-\tau_{ki_2})|^2\right\}. \tag{37}$$

For independent and uniform $\tau_{ki_1} \neq \tau_{ki_2}$, the pdf of $\delta = \tau_{ki_1} - \tau_{ki_2}$ is symmetric

$$f_\delta(x) = \int_0^{T_p} p_{\tau_{ki}}(x+\tau)p_{\tau_{ki}}(\tau)d\tau, \quad |x| < T_p$$
$$= \frac{e^{-T_p/T_0}}{T_0(1-e^{-T_p/T_0})^2}\cdot\sinh\left(\frac{T_p-|x|}{T_0}\right), \quad |x| < T_p. \tag{38}$$

Thus, two quantities can be defined and numerically

calculated:

$$\rho_1 = \mathrm{E}\{|R_p(\tau_{ki_1} - \tau_{ki_2})|^2\} = \int_0^{T_p} 2 f_\delta(x) |R_p(x)|^2 dx, \tag{39a}$$

$$\rho_{1,e} = \mathrm{E}\left\{\left|R_p(T_p - T_e - \tau_{kj} + \tau_{e,ki})\right|^2\right\} = \int_{-T_p}^{T_p} f_\delta(x) \left|R_p(T_p - T_e + x)\right|^2 dx. \tag{39b}$$

Therefore,

$$\begin{aligned}\mathrm{E}\{Q_{d1}\} &= \sigma_B^2 \left(\frac{1}{L}\sum_{L_k=0}^{L-1}\sqrt{L_k+1}\right)^2 \sum_{k_1}\sum_{k_2\neq k_1} b_{k1}b_{k2} + \sigma_B^2 \sum_k b_k^2 \left(\frac{3+L}{2}\right) + \frac{\sigma_B^2\rho_1}{L}\sum_k b_k^2 \sum_{L_k=0}^{L-1} L_k \\ &= \sigma_B^2 \left(\frac{1}{L}\sum_{L_k=0}^{L-1}\sqrt{L_k+1}\right)^2 \sum_{k_1}\sum_{k_2\neq k_1} b_{k1}b_{k2} + \sigma_B^2 \left(\frac{3+L}{2}\right) + \frac{\sigma_B^2\rho_1(L-1)}{2}.\end{aligned} \tag{40a}$$

On the other hand, for the unintended receiver

$$\begin{aligned}\mathrm{E}\{Q_{e1}\} &= \mathrm{E}\left\{\sum_k \beta_k^2 \sum_{i,j} \sigma_B^2\sigma_E^2 |R_p(T_p - T_e - \tau_{kj} + \tau_{e,ki})|^2\right\} \\ &= \sigma_E^2\rho_{1,e}\sum_k b_k^2 \frac{1}{L}\sum_{L_k=0}^{L-1}(L_k+1) = \sigma_E^2\rho_{1,e}\cdot\left(\frac{L+1}{2}\right).\end{aligned} \tag{40b}$$

### B. Direct Transmission Analysis

For direct transmission, first define

$$\rho_2 = \mathrm{E}\left\{\left|R_p(\tau_{ki})\right|^2\right\} = \int_0^{T_p} p_{\tau_{ki}}(x)\left|R_p(x)\right|^2 dx, \tag{41a}$$

$$\rho_{2,e} = \mathrm{E}\left\{\left|R_p(T_p - T_{e0} + \tau_{e,ki})\right|^2\right\} = \int_0^{T_p} p_{\tau_{ki}}(x)|R_p(T_p - T_{e0} + x)|^2 dx. \tag{41b}$$

Accordingly,

$$\begin{aligned}\mathrm{E}\{Q_{d2}\} &= \mathrm{E}\left\{\sum_k {b_k}^2 \sum_{i=0}^{L_k} \sigma_B^2 \left|R_p(\tau_{ki})\right|^2\right\} \\ &= \sum_k {b_k}^2 \sigma_B^2 \frac{1}{L}\sum_{L_k=0}^{L-1}\sum_{i=0}^{L_k} \mathrm{E}\left\{\left|R_p(\tau_{ki})\right|^2\right\} \qquad (42a) \\ &= \rho_2\sigma_B^2 \frac{1}{L}\sum_{L_k=0}^{L-1}(L_k+1)\sum_k {b_k}^2 = \frac{\rho_2\sigma_B^2(L+1)}{2}, \qquad (42b)\end{aligned}$$

$$\begin{aligned}\mathrm{E}\{Q_{e2}\} &= \mathrm{E}\left\{\sum_k {b_k}^2 \sum_{i=0}^{L_k} \sigma_E^2 \left|R_p(T_p - T_{e0} + \tau_{e,ki})\right|^2\right\} \\ &= \sum_k {b_k}^2 \sigma_E^2 \frac{1}{L}\sum_{L_k=0}^{L-1}\sum_{i=0}^{L_k} \mathrm{E}\left\{\left|R_p(T_p - T_{e0} + \tau_{e,ki})\right|^2\right\} \qquad (42c) \\ &= \rho_{2,e}\sigma_E^2 \frac{1}{L}\sum_{L_k=0}^{L-1}(L_k+1)\sum_k {b_k}^2 = \frac{\rho_{2,e}\sigma_E^2(L+1)}{2}. \qquad (42d)\end{aligned}$$

### C. Distributed Beamforming Analysis

Based on our previous analysis,

$$\rho_3 = \mathrm{E}\{|R_p(\tau_{ki} - \tau_{k0})|^2\} = \int_{-T_p}^{T_p} f_\delta(x)|R_p(x)|^2 dx, \tag{43a}$$

$$\rho_{3,e} = \mathrm{E}\left\{\left|R_p(T_p - T_{e1} - \tau_{k0} + \tau_{e,ki})\right|^2\right\} = \int_{-T_p}^{T_p} f_\delta(x)|R_p(T_p - T_{e1} + x)|^2 dx. \tag{43b}$$

Thus, for LoS-DBF, $i_0 = 0$, resulting in

$$\begin{aligned}\mathrm{E}\{Q_{d3}\} &= \frac{1}{K}\sum_k \left(\frac{1}{L}\sum_{L_k=0}^{L-1}\sum_{i\neq 0}^{L_k} \sigma_B^2 \mathrm{E}\left\{|R_p(\tau_{ki} - \tau_{k0})|^2\right\}\right) + \sigma_B^2(K+1) \\ &= \sigma_B^2\rho_3\left(\frac{L-1}{2}\right) + \sigma_B^2(K+1),\end{aligned} \tag{44a}$$

$$\begin{aligned}\mathrm{E}\{Q_{e3}\} &= \frac{1}{K}\sum_k \left(\frac{1}{L}\sum_{L_k=0}^{L-1}\sum_{i}^{L_k} \sigma_E^2 \cdot \mathrm{E}\left\{|R_p(T_p - T_{e1} - \tau_{k0} + \tau_{e,ki})|^2\right\}\right) \\ &= \frac{\sigma_E^2\rho_{3,e}(L+1)}{2}.\end{aligned} \tag{44b}$$

In MGP-DBF, $i_0$ is random and

$$\begin{aligned}\mathrm{E}\{Q_{d4}\} &= K^{-1}\sigma_B^2 \sum_k \frac{1}{L}\sum_{L_k=0}^{L-1}\sum_{i\neq i_0}^{L_k} \mathrm{E}\{|R_p(\tau_{ki} - \tau_{ki_0})|^2\} + \frac{\sigma_B^2}{L}\sum_{L_k=0}^{L-1}[(K-1) + G_1(L_k)]\,G_0(L_k) \\ &= K^{-1}\sigma_B^2 \sum_k \frac{1}{L}\sum_{L_k=0}^{L-1}\sum_{i\neq i_0}^{L_k} \rho_4 + \frac{\sigma_B^2}{L}\sum_{L_k=0}^{L-1}[(K-1) + G_1(L_k)]\,G_0(L_k) \\ &= \frac{\sigma_B^2}{L}\left[\rho_4\frac{L(L-1)}{2} + (K-1)\sum_{L_k=0}^{L-1} G_0(L_k) + \sum_{L_k=0}^{L-1} G_1(L_k)G_0(L_k)\right],\end{aligned} \tag{45a}$$

$$\mathrm{E}\{Q_{e4}\} = K^{-1}\sigma_E^2 \sum_k \frac{1}{L} \sum_{L_k=0}^{L-1} \left( \sum_{i=0}^{L_k} E\left\{ |R_p(T_p - T_{e1} - \tau_{ki_0} + \tau_{e,ki})|^2 \right\} \right) = \frac{\sigma_E^2 \rho_{4,e}(L+1)}{2}, \quad (45b)$$

where

$$\rho_4 = \mathrm{E}\{|R_p(\tau_{ki} - \tau_{ki_0})|^2\} = \rho_3, \quad (45c)$$

$$\rho_{4,e} = \mathrm{E}\left\{ \left| R_p(T_p - T_{e1} - \tau_{ki_0} + \tau_{e,ki}) \right|^2 \right\} = \int_{-T_p}^{T_p} f_\delta(x) |R_p(T_p - T_{e1} + x)|^2 dx. \quad (45d)$$

### D. Performance Comparison

Based on the above analysis, and when the noise levels at the destination and the unintended receiver are assumed identical such that $\sigma_n^2 = \sigma_e^2$, the SNRs of different transmission schemes at the destination and unintended receiver can be compared to illustrate PHY secrecy enhancement [25], by using the SNR gap between desired destination and eavesdropper, denoted in dB as $\mathrm{SNR}_{gap} = \mathrm{SNR}_d - \mathrm{SNR}_e$. The performance of the various schemes under consideration can be compared under different conditions.

## VI. Numerical Results and Examples

Numerical results are now presented to compare the performance of four different transmission schemes in terms of SNR gap (or secrecy rate): DTR, DT, LoS-DBF, and MGP-DBF. By varying the multi-path profiles of the source-to-destination channels and source-to-unintended-receivers, both fixed and random channel multi-path number $L_k$ can be tested.

First, the two channels in the non-degraded wiretapping scenario [17], [18] are assumed to be i.i.d. with equal variance $\sigma_B^2 = \sigma_E^2 = 0.4$ mW, and equal noise power $\sigma_n^2 = \sigma_e^2 = 0.1$ mW. Throughout the simulation, a RRC pulse shape with roll-off factor of $\alpha = 0.2$ was used [15]. In the various graphs presented, the suffix "$-t$" or solid lines are used to label theoretical results, whereas the suffix "$-n$" or dotted lines are used to label numerical results for the four different schemes under comparison. For the exponential multiplath power delay profile, the parameter $T_0 = T$ is used without loss of generality and $T_p = 2T$.[1]

In terms of the sampling instant at the unintended receiver node, let $T_e = T_{e0} = T_{e1} = T_p + \Delta$, where $\Delta$ is the sampling time offset. Two cases are tested: $\Delta = 0$ and uniform $\Delta$ on $(-0.5T, 0.5T)$. The first case gives the unintended receivers the benefit of the doubt such that they sample at the same moment $\ell T + T_e = \ell T + T_p$ as the target receiver. The second case takes into account the timing uncertainty, such that the unintended receivers may sample uniformly within $(-0.5T, 0.5T)$ of the sampling instants $\ell T + T_p$ at the target receivers, which is a typical case in practice.

[1]For a uniform multi-path delay profile, the decay time is set as $T_0 = \infty$.

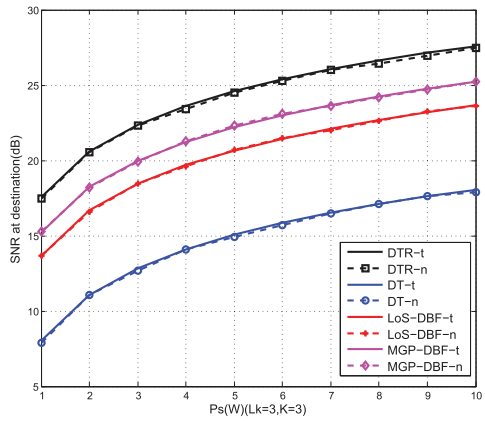


(a) Received signal SNR at target;

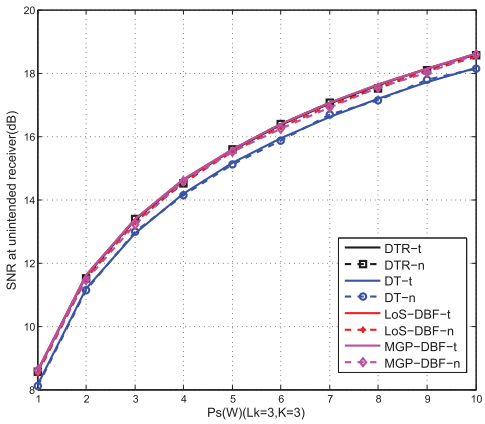


(b) SNR at unintended receiver $\Delta = 0$;

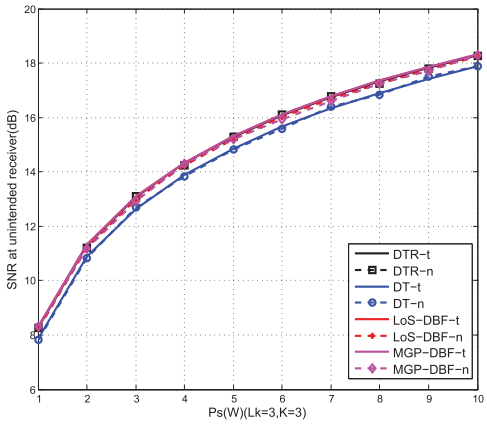


(c) SNR at unintended receiver (uniform $\Delta$).

Fig. 2. Received signal SNR results for ($L_k = 3$, $K = 3$). For uniform $\Delta \in (-0.5T, 0.5T)$, 1000 Monte Carlo random sampling instants were tested.

### A. Fixed Multi-Path Number $L_k$

In this case, the received SNR for different schemes is assessed while fixing the number of transmit antennas $K$ and the number of multi-paths $L_k$, for various levels of transmit power $P_s$. For numerical results, 1000 random multi-path channels and delays were generated for Monte Carlo evaluation.

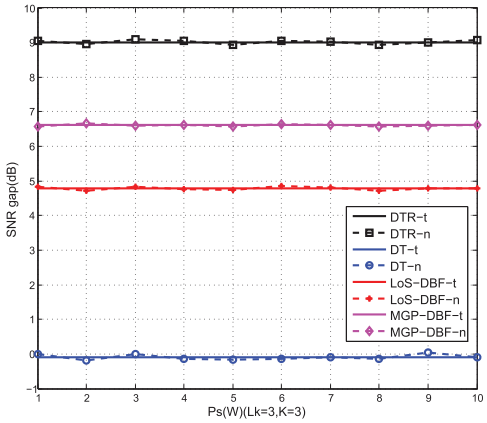


(a) Received signal SNR gap;

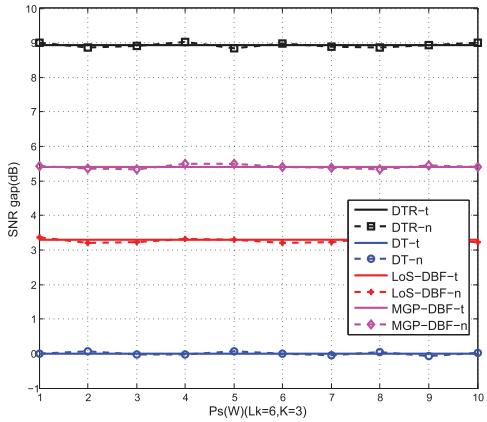


(b) Received signal SNR gap.

Fig. 3. Comparison of SNR gaps between target and unintended receivers for $L_k = 3$ and $L_k = 6$, $K = 3$, $\Delta = 0$.

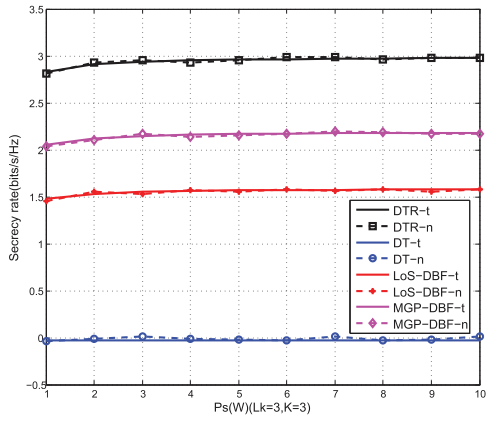


(a) Secrecy rate;

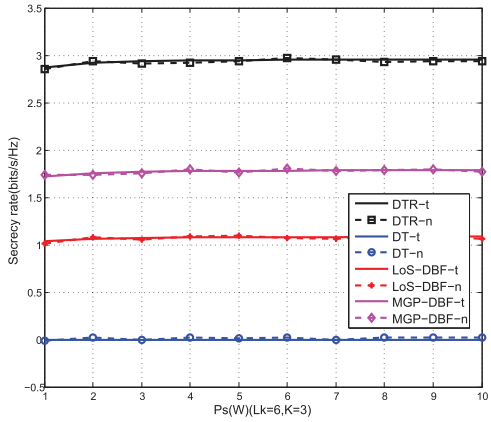


(b) Secrecy rate.

Fig. 4. Secrecy rates at destination and unintended receivers for $L_k = 3$ and $L_k = 6$, $K = 3$, $\Delta = 0$.

Fig. 2 shows both the theoretical and numerical results at different power levels $P_s$ for $L_k = 3$. The SNR of DTR-based transmission, DT, LoS-DBF, and MGP-DBF are evaluated. As is expected from the analytical expression of the SNR results, the SNR increases linearly with $P_s$. Hence, when the power $P_s$ grows, the SNRs for all four schemes increase as shown in Fig. 2. Note that the horizontal axis representing $P_s$ has a linear scale, whereas the vertical axis representing SNR has a logarithmic scale. Close agreement is observed between analytical and numerical results for all four schemes. In order of performance, DTR achieves the highest SNR, with MGP and LoS beamforming trailing behind, followed by the least effective strategy of DT without considering the multi-path effect or the advantage of beamforming. On the other hand, when comparing the SNR at the unintended receivers, the received SNR is nearly identical in all four transmission strategies.

It is also clear that by letting $T_e = T_p$ which gives the benefit of the doubt to the unintended receivers in terms of symbol timing, the unintended receivers can see an approximately 0.3 dB SNR increase. Nevertheless, this slight change does not negate the significant SNR improvement as seen by the target receiver at the destination.

Similar results can also be obtained for different numbers of multi-paths, e.g., $L_k = 6$. Fig. 3 compares the SNR gap of various transmission schemes for $L_k = 3$ and 6, respectively. Since the SNR for both nodes linearly grow with $P_s$, it is not surprising that the SNR gap remains flat for all four schemes. Among the four transmission schemes, DTR-based transmission provides the biggest SNR-gap between the destination node and unintended receivers. In fact, DTR is better than the MGP-DBF scheme which has a quite high complexity. This proves the simplicity and benefit of DTR transmission. Comparing the results of Fig. 3(a) and Fig. 3(b), observe the effect of the number of multi-path components. Assuming perfect receivers, as the number of multi-path components $L_k$ grows from 3 to 6, the SNR gap of DTR remains nearly unchanged while the SNR gaps of LoS-DBF and MGP-DBF decrease. This effect is reasonable and expected. The observed performance loss in beamforming is due to the relative reduction of signal energy in either the LoS path or the maximum gain path when the number of signal paths $L_k$ grows. On the other hand, DTR is robust to such uncertainties. In terms of corresponding secrecy rates, Fig. 4 illustrates similar results.

### *B. Random Number of Multi-Path Components*

In practical applications, the number of multi-path components, $L_k$, is uncertain and often time-varying. To obtain

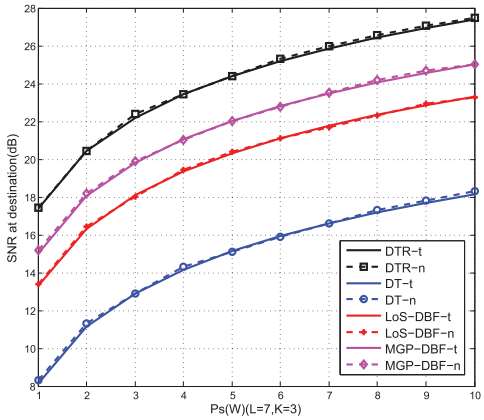


(a) Sampled signal SNR at target;

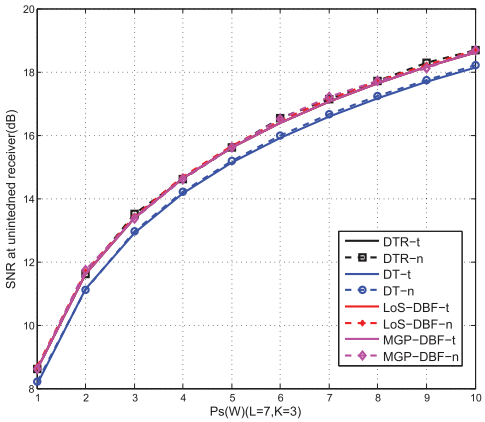


(b) SNR at unintended receiver $\Delta = 0$;

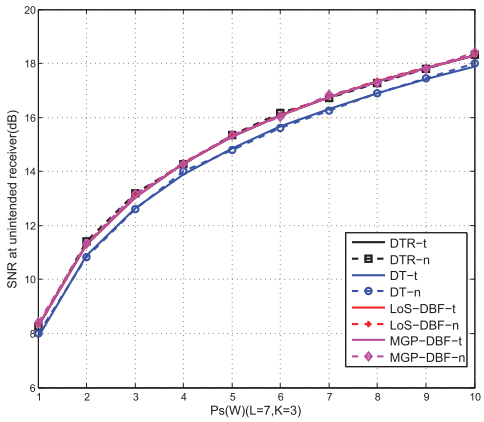


(c) SNR at unintended receiver (uniform $\Delta$).

Fig. 5. Received signal SNR comparison at different signal power $P_s$ for $L = 7$ and $K = 3$.

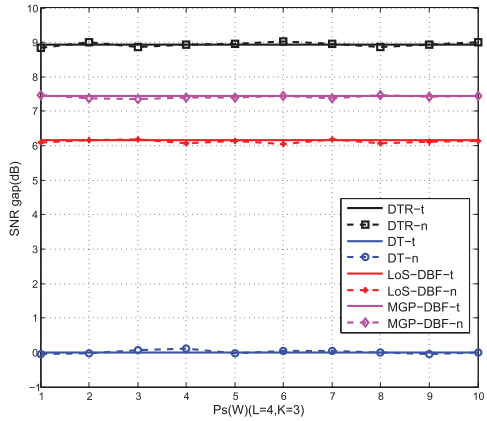


(a) Received signal SNR gap;

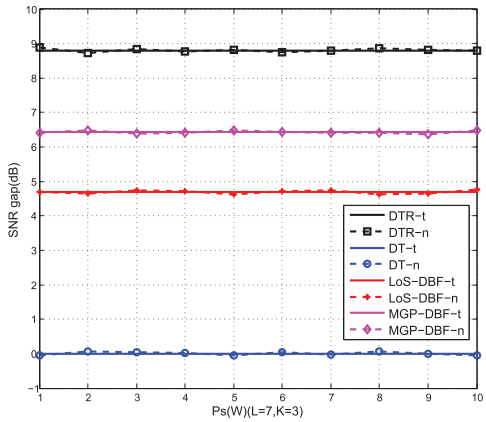


(b) Received signal SNR gap.

Fig. 6. Received SNR gaps for multi-path length $L = 4$ and $L = 7$, respectively, for $K = 3$, $\Delta = 0$.

numerical results for such cases, 3000 random multi-path channels and delays were generated in Monte Carlo evaluation, for which $L_k$ was assumed to be uniformly distributed in $\{0, \ldots, L-1\}$. All other parameters remain unchanged from the previous section.

Fig. 5 presents theoretical and numerical SNR results for different power levels $P_s$, given $L = 7$ and $K = 3$. The results compare the SNR of DTR transmission, direct transmission (DT), LoS-DBF, and MGP-DBF. Once again, close agreement is observed between the analytical and numerical results for all four schemes. From the analytical expression for the SNR in Sect. V, the linear SNR growth with $P_s$ is confirmed. Again, notice that the horizontal axis representing $P_s$ has a linear scale, whereas the vertical axis representing SNR has a logarithmic scale. Similar to the case of fixed $L_k$, the DTR transmission leads to the highest destination SNR and better signal quality. Likewise, by giving unintended receivers the benefit of the doubt in terms of symbol timing, $\Delta = 0$ implies $T_e = T_p$. Compared with random $\Delta$, the sampled signal SNR at the unintended receiver is only marginally higher.

Fig. 6 illustrates the SNR gap between the destination and unintended receivers for four different schemes for $K = 3$ and $L = 4,\ 7$. Clearly, the SNR gap for DTR transmission is superior to that of three other schemes. Consistent with the previous results, for fixed $L_k$, DTR is robust to the distribution of the number of multi-path components, $L$. On the other hand, when the number of multi-path components grows, MGP-DBF and LoS-DBF provide less signal quality advantage at the destination receiver in terms of the SNR gap. The corresponding secrecy rates of Fig. 7 show similar results.

Next, the impact of the number of transmit antennas, $K$, on the SNR gap of the different schemes is studied. Fig. 8 presents

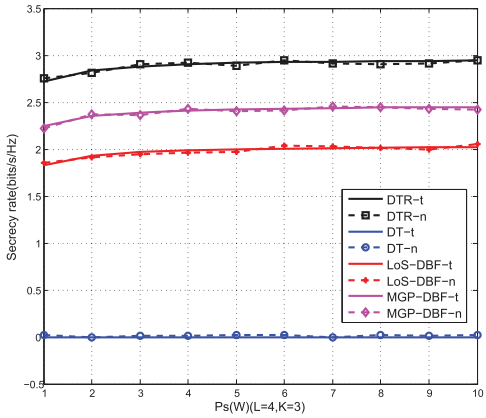


(a) Secrecy rate;

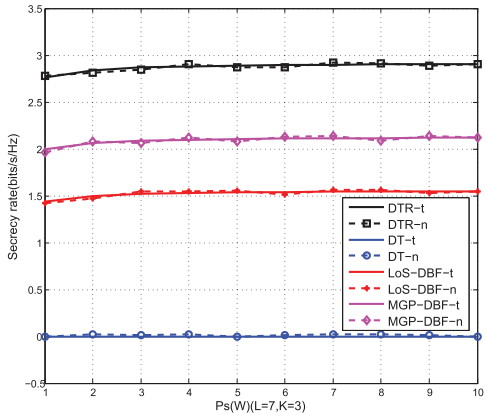


(b) Secrecy rate.

Fig. 7. Secrecy rates for multi-path length $L = 4$ and $L = 7$, respectively, for $K = 3$, $\Delta = 0$.

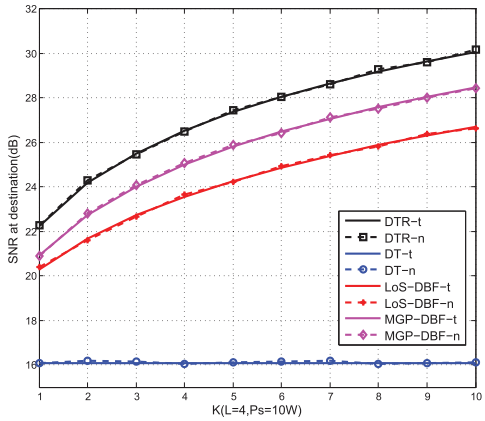


(a) Sampled signal SNR at destination;

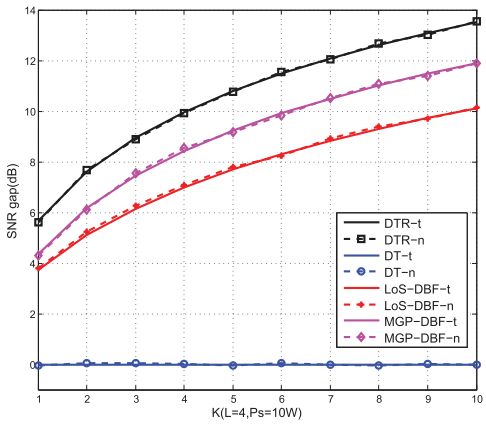


(b) Received signal SNR gap;

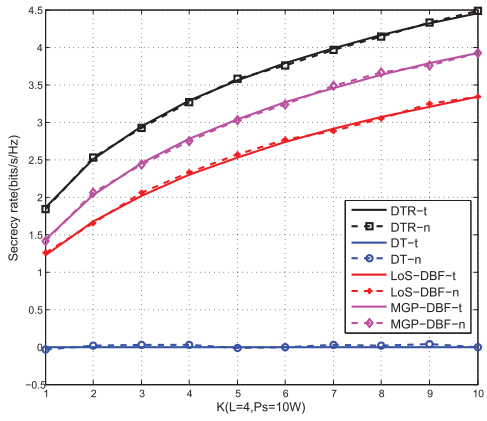


(c) Secrecy rate.

Fig. 8. Test results for $K$ distributed antennas ($L = 4$, $P_s = 10$W) and $\Delta = 0$.

the SNR result at the destination receiver and the SNR gap for $L = 4$ and $P_s = 10$ W. Similar to earlier cases, the theoretical results agree well with the real simulation results. Not surprisingly, as the number of distributed antennas $K$ increases, the SNR gaps for all three diversity transmission schemes increase. However, for DT, each antenna sends exactly the same pulse-shape without exploiting the diversity of the channels. As a result, a large number of distributed antennas fails to help elevate the SNR gap in direct transmission. Thus, the SNR gap for the direct transmission scheme is almost unchanged with increasing antenna diversity order $K$, while the SNR gap for other three schemes grow significantly for larger $K$. Overall, the SNR gap (and secrecy rate) for the DTR transmission scheme dominates the other three schemes. With respect to the impact of the temporal energy focusing effect by DTR, even with only $K = 2$ antennas the DTR-transmission scheme can achieve a SNR gap that is only achievable by MGP-DBF with $K = 4$ antennas or LoS-DBF with $K = 5$ antennas.

It was shown earlier that multi-path delay spread has a positive impact on DTR-based transmission, whereas the opposite is true for beamforming. This effect is illustrated more clearly by presenting another set of results where $L$ is varied. Fig. 9 compares the SNR gaps and the secrecy rates for different values of $L$, to assess the effect of multi-path delay spread. Clearly, as $L$ becomes larger, the SNR gaps for the DTR transmission and direct transmission schemes remain steady, while the SNR gaps for the remaining two DBF schemes decrease. Once again, the beamforming schemes suffer a larger performance loss as $L$ grows, because the beamforming relies on one path (either dominant or LoS). As the number of multi-paths grows, the strength of a single path becomes relatively weaker. Hence, beamforming will increasingly rely on weaker multi-path channel gains $h_{i_0,k}$. As a result, the performance of the DBF strategies degrades as $L$ becomes larger.

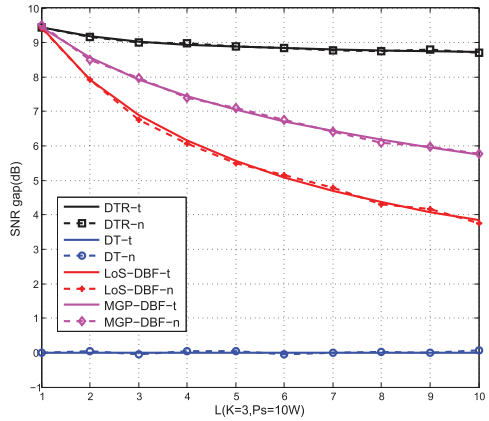


(a) Received SNR gap;

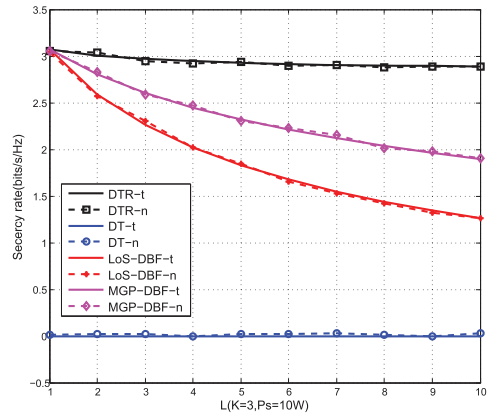


(b) Secrecy rate.

Fig. 9. SNR gap and secrecy rate comparison for ($K = 3$, $P_s = 10$ W) and variable $L$.

## VII. Conclusions

This paper analyzed the ability of distributed time-reversal (DTR) transmission to protect against unintended signal leakage to eavesdroppers. In DTR transmission, each transmit antenna individually exploits its local CSI and utilizes time-reversal to focus signal energy at the destination receiver, by exploiting its multi-path channel to the destination receiver. The performance of DTR-based transmission, direct transmission, LoS distributed beamforming and MGP distributed beamforming were analyzed and compared with respect to signal leakage, as measured by the SNR gap between the destination and unintended receivers. Numerical results were presented that demonstrate both the SNR improvement of the DTR-based transmission scheme and the validity of the performance analysis. Further, given multi-path channels, DTR transmission is a much more effective signaling strategy against signal leakage to unintended receivers than traditional beamforming strategies, particularly when the number of multi-path components is large.

## References

[1] G. Lerosey, J. de Rosny, A. Tourin, A. Derode, G. Montaldo, and M. Fink, "Time reversal of electromagnetic waves," *Phys. Rev. Lett.*, vol. 92, no. 19, pp. 193904-1–193904-3, May 2004.

[2] M. Emami, M. Vu, J. Hansen, A. J. Paulraj, and G. Papanicolaou, "Matched filtering with rate back-off for low complexity communications in very large delay spread channels," in *Proc. 38th Asilomar Conf. Signal Syst. Comput.*, Nov. 2004, pp. 218–222.

[3] C. Oestges, A. D. Kim, G. Papanicolaou, and A. J. Paulraj, "Characterization of space-time focusing in time-reversed random fields," *IEEE Trans. Antennas Propag.*, vol. 53, no. 1, pp. 283–293, Jan. 2005.

[4] H. T. Nguyen, I. Z. Kovacs, and P. C. F. Eggers, "A time reversal transmission approach for multiuser UWB communications," *IEEE Trans. Antennas Propag.*, vol. 54, no. 11, pp. 3216–3224, Nov. 2006.

[5] H. El-Sallabi, P. Kyritsi, A. Paulraj, and G. Papanicolaou, "Experimental investigation on time reversal precoding for space-time focusing in wireless communications," *IEEE Trans. Instrum. Meas.*, vol. 59, no. 6, pp. 1537–1543, Jun. 2010.

[6] D. Li, J. S. Hong, and B. Wang, "Improving anti-detection/interception performance for wireless sensor network based on time-reversal technology," in *Proc. 5th Int. Conf. Wireless Commun. Netw. Mobile Comput. (Wicom)*, Beijing, China, Sep. 2009, pp. 1–4.

[7] D. T. Phan-Huy, S. Ben Halima, and M. Helard, "Dumb-to-perfect receiver throughput ratio maps of a time reversal wireless indoor system," in *Proc. 20th Int. Conf. Telecommun. (ICT)*, Casablanca, Morocco, May 2013 pp. 1–5.

[8] F. Renna, N. Laurenti, and H. V. Poor, "Physical-layer secrecy for OFDM transmissions over fading channels," *IEEE Trans. Inf. Forensics Secur.*, vol. 7, no. 4, pp. 1354–1367, Aug. 2012.

[9] Y. Yang, Q. Li, W.-K. Ma, J. Ge, and P. C. Ching, "Cooperative secure beamforming for AF relay networks with multiple eavesdroppers," *IEEE Signal Process. Lett.*, vol. 20, no. 1, pp. 35–38, Jan. 2013.

[10] K. A. Toshiaki, A. F. Molisch, C. Duan, Z. Tao, and P. Orlik, "Capacity, MSE and secrecy analysis of linear block precoding for distributed antenna systems in multi-user frequency-selective fading channels," *IEEE Trans. Commun.*, vol. 59, no. 3, pp. 888–900, Jan. 2011.

[11] D. T. Phan-Huy, T. Sarrebourse, A. Gati, J. Wiart, and M. Helard, "Characterization of the confidentiality of a green time reversal communication system: Experimental measurement of the spy BER sink," in *Proc. IEEE Wireless Commun. Netw. Conf. (WCNC)*, Shanghai, China, Apr. 2013, pp. 4783–4788.

[12] P. Blomgren, K. Persefoni, A. D. Kim, and G. Papanicolaou, "Spatial focusing and intersymbol interference in multiple-input single-output time reversal communication systems," *IEEE J. Ocean. Eng.*, vol. 33, no. 3, pp. 341–355, Oct. 2008.

[13] H. Nguyen, Z. Zhao, F. Zheng, and T. Kaiser, "Preequalizer design for spatial multiplexing SIMO-UWB TR systems," *IEEE Trans. Veh. Technol.*, vol. 59, no. 8, pp. 3798–3805, Oct. 2010.

[14] B. Wang, Y. Wu, F. Han, Y. H. Yang, and K. Liu, "Green wireless communications: A time-reversal paradigm," *IEEE J. Sel. Areas Commun.*, vol. 29, no. 8, pp. 1698–1710, Sep. 2011.

[15] G. L. Stüber, *Principles of Mobile Communication*. New York, NY, USA: Springer, 2012.

[16] M. S. Kim, M. Yoon, and C. Lee, "Performance analysis of a frequency-domain equal-gain-combining time-reversal scheme for distributed antenna systems," *IEEE Commun. Lett.*, vol. 16, no. 9, pp. 1454–1457, Sep. 2012.

[17] A. D. Wyner, "The wire-tap channel," *Bell Syst. Tech. J.*, vol. 54, no. 8, pp. 1355–1387, Oct. 1975.

[18] I. Csiszar and J. Korner, "Broadcast channels with confidential messages," *IEEE Trans. Inf. Theory*, vol. IT-24, no. 3, pp. 339–348, May 1978.

[19] L. Wang and H. Wu, "Jamming partner selection for maximising the worst D2D secrecy rate based on social trust," *Trans. Emerging Telecommun. Technol.*, Oct. 2015, pp. 1–11, doi: 10.1002/ett.2992.

[20] K. K. Borah, R. A. Kennedy, Z. Ding, and I. Fijalkow, "Sampling and prefiltering effects on blind equalizer design," *IEEE Trans. Signal Process.*, vol. 49, no. 1, pp. 209–218, Jan. 2001.

[21] G. D. Forney, "Maximum-likelihood sequence estimation of digital sequences in the presence of intersymbol interference," *IEEE Trans. Inf. Theory*, vol. IT-18, no. 3, pp. 363–378, May 1972.

[22] J. Salz, "Optimum mean-square decision feedback equalization," *Bell Syst. Tech. J.*, vol. 52, no. 8, pp. 1341–1373, Oct. 1973.

[23] T. K. Y. Lo, "Maximum ratio transmission," *IEEE Trans. Commun.*, vol. 47, no. 10, pp. 1458–1461, Oct. 1999.

[24] H. A. David and H. N. Nagaraja, *Order Statistics*, 3rd ed. Hoboken, NJ, USA: Wiley, 2005.

[25] L. Wang, L. Yang, X. Ma, and M. Song, "Security-oriented cooperation scheme in wireless cooperative networks," *IET Commun.*, vol. 8, no. 8, pp. 1265–1273, May 2014.

**Li Wang** (S'08–M'14–SM'16) received the Ph.D. degree from Beijing University of Post and Telecommunications (BUPT), Beijing, China, in 2009. She currently serves as an Associate Professor with the School of Electronic Engineering, BUPT, where she leads the Laboratory of High Performance Computing and Networking. From December 2013 to January 2015, she held a Visiting Research position at the School of Electrical and Computer Engineering, Georgia Tech, Atlanta, GA, USA. From August 2015 to November 2015, she held a Visiting Researcher position at the Department of Signals and Systems, Chalmers University of Technology, Gothenburg, Sweden. Her research interests include wireless networking, secure communications, distributed storage system, device-to-device communication systems, and peer-to-peer networks. She has been serving as a SWAT Team member for the IEEE TRANSACTIONS ON VEHICULAR TECHNOLOGY since January 2016, and also served on the technical program committees of the IEEE CCNC 2009, IEEE CCNC 2010, IEEE WCSP 2013, IEEE GLOBECOM 2014, IEEE WCNC 2015, IEEE ICC 2015, IEEE ICNC 2015, IEEE ICCC 2015, IEEE GLOBECOM 2015, IEEE ICNC 2016, and IEEE ICC 2016. She was the recipient of 2013 Beijing Young Elite Faculty for Higher Education Award, Best Paper Award and Best Paper Runner Up from ICCTA 2011 and WASA 2015, respectively.

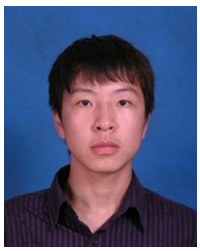

**Ruoguang Li** (S'15) received the bachelor's degree from Nanjing University of Posts and Telecommunications (NUPT), Nanjing, China, in 2013. He is currently pursuing the Ph.D. degree at the School of Electronic Engineering, Beijing University of Posts and Telecommunications (BUPT), Beijing, China. His research interests include wireless communications with current focus on physical layer security, cooperative networks.

**Chunyan Cao** received the B.S. and M.S. degrees from Beijing University of Posts and Telecommunications (BUPT), Beijing, China, in 2012 and 2015, respectively. Her research interests include cooperative networking, and physical layer security.

**Gordon L. Stüber** (S'81–M'82–SM'96–F'99) received the B.A.Sc. and Ph.D. degrees in electrical engineering from the University of Waterloo, Waterloo, ON, Canada, in 1982 and 1986, respectively. In 1986, he joined the School of Electrical and Computer Engineering, Georgia Institute of Technology, Atlanta, GA, USA, where he is the Joseph M. Pettit Chair Professor of communications. He is the author of the wireless textbook *Principles of Mobile Communication* (Kluwer Academic Publishers, 1996, 2/e 2001, 3/e 2011). He was the corecipient of the Jack Neubauer Memorial Award in 1997 for the Best Systems Paper published in the IEEE TRANSACTIONS ON VEHICULAR TECHNOLOGY. He was the recipient of the IEEE Vehicular Technology Society James R. Evans Avant Garde Award in 2003 "for his contributions to theoretical research in wireless communications." In 2007, he was also the recipient of the IEEE Communications Society Wireless Communications Technical Committee Recognition Award (2007) "for outstanding technical contributions in the field and for service to the scientific and engineering communities." He was the Distinguished Lecturer of the IEEE Communication Society (2007–2008) and the IEEE Vehicular Technology Society (2010–2012). Finally, he was the corecipient of the Neal Shepherd Memorial Best Propagation Paper Award in 2012, for the best propagation paper published in the IEEE TRANSACTIONS ON VEHICULAR TECHNOLOGY.

Dr. Stüber served as the Technical Program Chair for the 1996 IEEE Vehicular Technology Conference (VTC'96), the Technical Program Chair for the 1998 IEEE International Conference on Communications (ICC'98), the General Chair of the Fifth IEEE Workshop on Multimedia, Multiaccess, and Teletraffic for Wireless Communications (MMT'2000), the General Chair of the 2002 IEEE Communication Theory Workshop (CTW'02), and the General Chair of the Fifth YRP International Symposium on Wireless Personal Multimedia Communications (WPMC'2002). He is a past Editor for Spread Spectrum with the IEEE TRANSACTIONS ON COMMUNICATIONS (1993–1998), and a past member of the IEEE Communications Society Awards Committee (1999–2002). He served as an elected Member-at-Large on the IEEE Communications Society Board of Governors (2007–2009), and is currently an elected member of the IEEE Vehicular Technology Society Board of Governors (2001–2018). He was the recipient the IEEE Vehicular Technology Society Outstanding Service Award in 2005.